Tiitinen, Lauri; Martin, Floran; Hinkkanen, Marko; Harnefors, Lennart

Current-regulated V/Hz control of induction motors

Published in:
2022 International Conference on Electrical Machines (ICEM)

DOI:
10.1109/ICEM51905.2022.9910621

Published: 13/10/2022

Document Version
Peer-reviewed accepted author manuscript, also known as Final accepted manuscript or Post-print

Please cite the original version:
Tiitinen, L., Martin, F., Hinkkanen, M., & Harnefors, L. (2022). Current-regulated V/Hz control of induction motors. In *2022 International Conference on Electrical Machines (ICEM)* (pp. 579-585). Article 9910621 (Proceedings (International Conference on Electrical Machines)). IEEE. https://doi.org/10.1109/ICEM51905.2022.9910621

Current-Regulated V/Hz Control of Induction Motors

Lauri Tiitinen, Floran Martin, Marko Hinkkanen, *Senior Member, IEEE*, and Lennart Harnefors, *Fellow, IEEE*

***Abstract*—This paper deals with current-regulated V/Hz control for induction motors. The analyzed control method incorporates an outer voltage control loop and an inner current control loop. Consequently, the stator current can be limited and unnecessary overcurrent trips avoided. Stability of the control system is analyzed by means of small-signal linearization. It is shown that the current-regulated V/Hz control has similar regions of instability as conventional V/Hz control. Static output feedback can be used to increase the stable operating region and improve system damping.**

***Index Terms*—Current limitation, induction machine, scalar control, stability.**

I. Introduction

In high-performance induction motor drive applications, field-oriented control schemes are the typical choice. For less demanding applications, the V/Hz-controlled drive remains a popular alternative, despite its inferior dynamic performance and reference-tracking capabilities. In many applications, however, the simplicity and ease of commissioning of the V/Hz control outweigh its drawbacks.

Due to its open-loop nature, the V/Hz control calls for the inclusion of two operating-point correcting measures, compensation for the stator resistance voltage drop and compensation for slip [1]. The former ensures the adequate production of flux, especially at low speeds, while the latter corrects the speed deviation originating from the load-dependent slip. Compensation strategies for the voltage drop in stator resistance include boosting the stator voltage at low speeds [2] and calculating the voltage drop dynamically from the stator resistance estimate and measured stator current [1]. The slip can be compensated for by altering the speed reference with a slip estimation based on either name plate data [3] or flux estimator [4].

In addition to these well-known operating point altering issues, the induction motor in open-loop control exhibits operating regions of poor dampening and small-signal instability [5], which arise from the nonlinear coupling between the electrical and mechanical subsystems [4]. These regions of instability are found in the mid-speed region under low and medium loads and in the low-speed region under heavy loads [4].

This work was supported in part by ABB Oy.

L. Tiitinen, M. Hinkkanen, and F. Martin are with the Department of Electrical Engineering and Automation, Aalto University, Espoo, Finland (e-mail: lauri.tiitinen@aalto.fi; floran.martin@aalto.fi; marko.hinkkanen@aalto.fi).

L. Harnefors is with ABB Corporate Research, Västerås, Sweden (e-mail: lennart.harnefors@se.abb.com).

For the unstable mid-speed region, static output feedback from the stator current is a common remedy, for which several numerical tuning approaches are found in the literature [6], [7]. Recently in [4], a more analytical, passivity-based approach is taken to mitigate the small-signal instability in the middle-speed region. The unstable low-speed region under heavy loads is of different nature and likely not stabilizable by means of V/Hz control and static feedback compensators [4].

Moreover, the limitation of stator current is troublesome in V/Hz control. While many modern V/Hz control methods utilize stator current measurement in their control algorithms, the current is not directly regulated. This severely complicates the performance of V/Hz control schemes in overload conditions as the safe operation of the inverter requires that the stator current is kept within its limits. Means to arrest a stator current surge in overload conditions are limited, often resulting in undesirable protection circuit trips. Conventionally, current limitation is achieved indirectly by decreasing the stator frequency or voltage when either the stator current or the estimated slip frequency reach their respective limits [8]. A current limitation method based on two proportional-integral (PI) controllers regulating both the stator voltage reference and the stator frequency reference is proposed in [9], but the mid-speed instability phenomena is disregarded. Furthermore, as the current is not directly controlled, an overcurrent trip may still occur.

In the method presented in [10], a current controller is applied to V/Hz control. In this control scheme, two control loops, an inner current control loop and an outer voltage control loop, are utilized to emulate the dynamics of the open-loop V/Hz-controlled induction motor drive. The presented method retains the benefits of V/Hz control desired in medium-performance applications, while the added current control loop improves operation during overload events.

In this paper, the current-regulated V/Hz control scheme presented in [10] is further studied by means of stability analysis, simulations, and experiments. The results are compared to open-loop V/Hz methods. It is shown that the current-controlled approach suffers from similar instability issues as open-loop V/Hz methods, with the unstable regions being comparable in size if not larger, depending on the tuning of the voltage controller. Furthermore, improvements and tuning guidelines for the current-regulated V/Hz control are proposed.

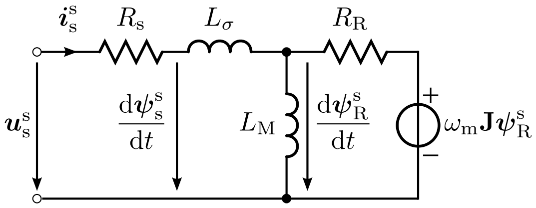

Fig. 1. Equivalent circuit of the induction motor in stator coordinates.

II. System Configuration

In this work, vector quantities are presented using real-valued column vectors, e.g. the stator current $\boldsymbol{i}_\mathrm{s} = [i_\mathrm{sd}, i_\mathrm{sq}]^\mathrm{T}$. Furthermore, block matrices, such as the identity matrix $\mathbf{I} = \left[\begin{smallmatrix}1 & 0\\ 0 & 1\end{smallmatrix}\right]$ and the orthogonal rotation matrix $\mathbf{J} = \left[\begin{smallmatrix}0 & -1\\ 1 & 0\end{smallmatrix}\right]$, are adopted for enhanced readability. Per-unit (p.u.) quantities are used in the analysis.

The standard inverse-Γ model is used to model the induction motor [11]. The equivalent circuit of the model is shown in Fig. 1. The stator current $\boldsymbol{i}_\mathrm{s}$ and the rotor flux linkage $\boldsymbol{\psi}_\mathrm{R}$ are chosen as the state variables and the state equations are represented in synchronous coordinates rotating at the stator angular frequency ω_s by

$$\begin{aligned} L_\sigma \frac{\mathrm{d}\boldsymbol{i}_\mathrm{s}}{\mathrm{d}t} &= -\left(R_\sigma \mathbf{I} + \omega_\mathrm{s} L_\sigma \mathbf{J}\right)\boldsymbol{i}_\mathrm{s} + \left(\alpha\mathbf{I} - \omega_\mathrm{m}\mathbf{J}\right)\boldsymbol{\psi}_\mathrm{R} + \boldsymbol{u}_\mathrm{s} \\ \frac{\mathrm{d}\boldsymbol{\psi}_\mathrm{R}}{\mathrm{d}t} &= R_\mathrm{R}\boldsymbol{i}_\mathrm{s} - (\alpha\mathbf{I} + \omega_\mathrm{r}\mathbf{J})\boldsymbol{\psi}_\mathrm{R} \end{aligned} \tag{1}$$

where $R_\sigma = R_\mathrm{s} + R_\mathrm{R}$ is the total resistance, $\boldsymbol{u}_\mathrm{s}$ is the stator voltage, $\alpha = R_\mathrm{R}/L_\mathrm{M}$ is the inverse rotor time constant, ω_m is the electrical angular speed of the rotor, and $\omega_\mathrm{r} = \omega_\mathrm{s} - \omega_\mathrm{m}$ is the slip angular frequency. The electromagnetic torque is given by

$$\tau_\mathrm{M} = \boldsymbol{i}_\mathrm{s}^\mathrm{T}\mathbf{J}\boldsymbol{\psi}_\mathrm{R} \tag{2}$$

and the mechanical subsystem is modeled as

$$J_\mathrm{m}\frac{\mathrm{d}\omega_\mathrm{m}}{\mathrm{d}t} = \tau_\mathrm{m} - \tau_\mathrm{L} \tag{3}$$

where J_m is the total moment of inertia and τ_L is the load torque.

III. Control System

Fig. 2 displays the control system, consisting of two loops. The inner loop regulates the stator current, while the outer loop controls the stator voltage.

The stabilization method presented for V/Hz control in [4] is adopted here for the current-regulated V/Hz control approach. The stabilizing feedback requires the operating-point stator current, which can be acquired by means of low-pass filtering the stator-current reference (the output of the voltage controller). The low-pass filter is governed by

$$\frac{\mathrm{d}\boldsymbol{i}_\mathrm{s,lpf}}{\mathrm{d}t} = \alpha_\mathrm{f}(\boldsymbol{i}_\mathrm{s,ref} - \boldsymbol{i}_\mathrm{s,lpf}) \tag{4}$$

where α_f is the filter bandwidth. Alternatively, the measured stator current could be used to calculate the operating-point stator current.

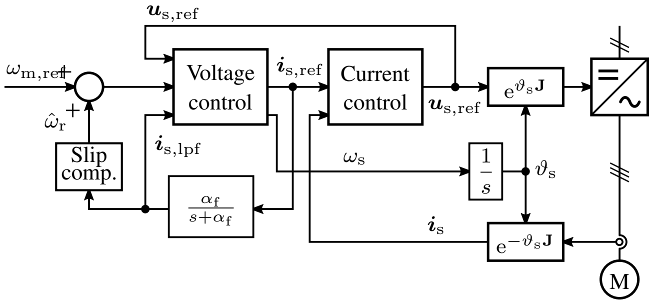

Fig. 2. Block diagram of the voltage-controlled current-regulated V/Hz control method.

A. Voltage Controller and Stator Frequency

The reference for the voltage controller resembles that of the V/Hz-controlled induction motor and is given by

$$\boldsymbol{u}_\mathrm{s,ref}' = R_\mathrm{s}\boldsymbol{i}_\mathrm{s,lpf} + \omega_\mathrm{s}\mathbf{J}\boldsymbol{\psi}_\mathrm{s,ref} + \boldsymbol{K}(\boldsymbol{i}_\mathrm{s,lpf} - \boldsymbol{i}_\mathrm{s,ref}) \tag{5}$$

where the first term is the RI compensation, $\boldsymbol{\psi}_\mathrm{s,ref} = [\psi_\mathrm{s,ref}, 0]^\mathrm{T}$ is a constant stator flux reference, ω_s is the internal stator frequency reference and the last term is a stabilizing feedback from high-pass-filtered stator current reference, where $\boldsymbol{K}$ is a 2×2 gain matrix. It should be noted, that the proportional part of the voltage controller originally in [10] is omitted here, as it would result in an algebraic loop in continuous time design.

The output of the voltage controller is the integral state $\boldsymbol{i}_\mathrm{s,ref}$ governed by

$$\frac{\mathrm{d}\boldsymbol{i}_\mathrm{s,ref}}{\mathrm{d}t} = k_\mathrm{v}(\boldsymbol{u}_\mathrm{s,ref}' - \boldsymbol{u}_\mathrm{s,ref}) \tag{6}$$

where k_v is the integral gain of the voltage controller and $\boldsymbol{u}_\mathrm{s,ref}$ is the output of the current controller.

The internal stator frequency is given by the voltage controller block as

$$\omega_\mathrm{s} = \omega_\mathrm{m,ref} + \hat{\omega}_\mathrm{r} + \boldsymbol{k}^\mathrm{T}(\boldsymbol{i}_\mathrm{s,lpf} - \boldsymbol{i}_\mathrm{s,ref}) \tag{7}$$

where $\omega_\mathrm{m,ref}$ is the rate-limited reference frequency given by the user, $\hat{\omega}_\mathrm{r}$ is the approximate slip frequency and the last term is a static stabilizing feedback from the stator current reference, where $\boldsymbol{k}$ is a 2×1 gain matrix. Orientation of the control coordinate system follows the stator flux reference angle calculated by integrating the stator frequency reference in (7).

The two gain matrices $\boldsymbol{K}$ and $\boldsymbol{k}$ function as injection points for altering the dynamics of the system. The gain matrices are selected according to the passivity-based gain design presented in [4], i.e.

$$\begin{aligned} \boldsymbol{K} &= -R_\mathrm{s}\mathbf{I} + kL_\sigma(\alpha\mathbf{I} + \omega_\mathrm{m}\mathbf{J}) \\ \boldsymbol{k} &= \frac{k_\omega R_\mathrm{R}\mathbf{J}\boldsymbol{\psi}_\mathrm{R0}}{\psi_\mathrm{R0}^2} \end{aligned} \tag{8}$$

where k and k_ω are a positive design parameters and $\boldsymbol{\psi}_{\mathrm{R0}}$ is the operating point rotor flux $\boldsymbol{\psi}_{\mathrm{R0}} = \boldsymbol{\psi}_{\mathrm{s,ref}} - L_\sigma \boldsymbol{i}_{\mathrm{s,lpf}}$. For the slip compensation, the slip frequency can be estimated as

$$\hat{\omega}_{\mathrm{r}} = \frac{R_{\mathrm{R}} \psi_{\mathrm{s,ref}} i_{\mathrm{sq}}}{\boldsymbol{\psi}_{\mathrm{R0}}^2} \tag{9}$$

It should be noted that compared to V/Hz control, the current-regulated V/Hz control method introduces several additional possible static output feedback injection points. In this paper, only stator voltage and frequency were used as injection points.

B. Current Controller

The PI-type current controller regulates the stator current to the reference given by the voltage controller. The output of the current controller is

$$\boldsymbol{u}_{\mathrm{s,ref}} = k_{\mathrm{p}} \boldsymbol{e} + \boldsymbol{w}_{\mathrm{i}} - r_{\mathrm{a}} \boldsymbol{i}_{\mathrm{s}} \tag{10}$$

where $\boldsymbol{e} = \boldsymbol{i}_{\mathrm{s,ref}} - \boldsymbol{i}_{\mathrm{s}}$. The integral state $\boldsymbol{w}_{\mathrm{i}}$ is governed by

$$\frac{\mathrm{d}\boldsymbol{w}_{\mathrm{i}}}{\mathrm{d}t} = k_{\mathrm{i}}(\boldsymbol{i}_{\mathrm{s,ref}} - \boldsymbol{i}_{\mathrm{s}}) \tag{11}$$

and the control gains are selected according to [12] as

$$\begin{aligned} r_{\mathrm{a}} &= \alpha_{\mathrm{c}} L_\sigma - R_{\mathrm{s}} \\ k_{\mathrm{p}} &= \alpha_{\mathrm{c}} L_\sigma \\ k_{\mathrm{i}} &= \alpha_{\mathrm{c}}^2 L_\sigma \end{aligned} \tag{12}$$

where α_{c} is the desired current control bandwidth.

IV. Analysis

A. Steady-state Operating Point

Stability of the nonlinear model in (1) can be analyzed by means of linearization. Here, operating point values are denoted with subscript 0. As a first step, the steady-state operating point is solved by substituting $\mathrm{d}/\mathrm{d}t = 0$. Three scalar quantities given as inputs are sufficient to uniquely define the operating point of the induction motor [4]. Here, the stator-flux magnitude ψ_{s0}, stator frequency ω_{s0} and the angular slip frequency ω_{r0} are chosen. The other operating-point quantities can be calculated using these, e.g. the operating-point stator current is obtained from (1) as

$$\boldsymbol{i}_{\mathrm{s0}} = \frac{\alpha \mathbf{I} + \omega_{\mathrm{r0}} \mathbf{J}}{R_{\mathrm{R}}} \boldsymbol{\psi}_{\mathrm{R0}} \tag{13}$$

The operating-point rotor flux can be solved as a function of stator flux by noting that $\boldsymbol{\psi}_{\mathrm{s0}} = L_\sigma \boldsymbol{i}_{\mathrm{s0}} + \boldsymbol{\psi}_{\mathrm{R0}}$ and applying (13),

$$\boldsymbol{\psi}_{\mathrm{R0}} = \frac{R_{\mathrm{R}}}{L_\sigma} \left(\omega_{\mathrm{rb}} \mathbf{I} + \omega_{\mathrm{r0}} \mathbf{J}\right)^{-1} \boldsymbol{\psi}_{\mathrm{s0}} \tag{14}$$

where $\omega_{\mathrm{rb}} = (1/L_{\mathrm{M}} + 1/L_\sigma) R_{\mathrm{R}}$ is the breakdown slip frequency. Finally, applying (13) to (2), the steady-state electromagnetic torque can be expressed as

$$\tau_{\mathrm{m0}} = \frac{\omega_{\mathrm{r0}}}{R_{\mathrm{R}}} \boldsymbol{\psi}_{\mathrm{R0}}^{\mathrm{T}} \boldsymbol{\psi}_{\mathrm{R0}} = \frac{\|\boldsymbol{\psi}_{\mathrm{R0}}\|^2 \omega_{\mathrm{r0}}}{R_{\mathrm{R}}} \tag{15}$$

B. Linearized Small-Signal Model

The local stability of the control method is studied by means of small-signal linearization. For simplicity, the inverter is assumed to be ideal, i.e., $\boldsymbol{u}_{\mathrm{s}} = \boldsymbol{u}_{\mathrm{s,ref}}$. Variables marked with δ denote the small-signal deviation about an operating point, as an example the small-signal stator current is $\delta \boldsymbol{i}_{\mathrm{s}} = \boldsymbol{i}_{\mathrm{s}} - \boldsymbol{i}_{\mathrm{s0}}$. The model in (1) is linearized as [4]

$$\begin{aligned} \frac{\mathrm{d}\delta \boldsymbol{x}_{\mathrm{m}}}{\mathrm{d}t} &= \underbrace{\begin{bmatrix} -\frac{R_\sigma}{L_\sigma}\mathbf{I} - \omega_{\mathrm{s0}}\mathbf{J} & \frac{1}{L_\sigma}\left(\alpha \mathbf{I} - \omega_{\mathrm{m0}}\mathbf{J}\right) \\ R_{\mathrm{R}}\mathbf{I} & -\alpha\mathbf{I} - \omega_{\mathrm{r0}}\mathbf{J} \end{bmatrix}}_{\boldsymbol{A}} \delta \boldsymbol{x}_{\mathrm{m}} \\ &+ \underbrace{\begin{bmatrix} \frac{1}{L_\sigma}\mathbf{I} \\ \mathbf{0} \end{bmatrix}}_{\boldsymbol{B}_{\mathrm{s}}} \delta \boldsymbol{u}_{\mathrm{s}} + \underbrace{\begin{bmatrix} -\mathbf{J}\boldsymbol{i}_{\mathrm{s0}} \\ -\mathbf{J}\boldsymbol{\psi}_{\mathrm{R0}} \end{bmatrix}}_{\boldsymbol{b}_{\mathrm{s}}} \delta \omega_{\mathrm{s}} + \underbrace{\begin{bmatrix} -\frac{1}{L_\sigma}\mathbf{J}\boldsymbol{\psi}_{\mathrm{R0}} \\ \mathbf{J}\boldsymbol{\psi}_{\mathrm{R0}} \end{bmatrix}}_{\boldsymbol{b}_{\mathrm{m}}} \delta \omega_{\mathrm{m}} \end{aligned} \tag{16a}$$

$$\delta \boldsymbol{i}_{\mathrm{s}} = \underbrace{\begin{bmatrix} \mathbf{I} & \mathbf{0} \end{bmatrix}}_{\boldsymbol{C}_{\mathrm{s}}} \delta \boldsymbol{x}_{\mathrm{m}} \tag{16b}$$

$$\delta \tau_{\mathrm{M}} = \underbrace{\begin{bmatrix} -\boldsymbol{\psi}_{\mathrm{R0}}^{\mathrm{T}}\mathbf{J} & \boldsymbol{i}_{\mathrm{s0}}^{\mathrm{T}}\mathbf{J} \end{bmatrix}}_{\boldsymbol{c}_{\mathrm{m}}} \delta \boldsymbol{x}_{\mathrm{m}} \tag{16c}$$

where $\delta \boldsymbol{x}_{\mathrm{m}} = \left[\delta \boldsymbol{i}_{\mathrm{s}}^{\mathrm{T}}, \delta \boldsymbol{\psi}_{\mathrm{R}}^{\mathrm{T}}\right]^{\mathrm{T}}$ is the state vector of the plant model.

The low-pass filter (4), the voltage controller (5), and current controller (10) are collected in matrix form, yielding

$$\begin{aligned} \frac{\mathrm{d}\delta \boldsymbol{x}_{\mathrm{c}}}{\mathrm{d}t} &= \underbrace{\begin{bmatrix} \mathbf{0} & k_{\mathrm{i}}\mathbf{I} & \mathbf{0} \\ -k_{\mathrm{v}}\mathbf{I} & -k_{\mathrm{v}}k_{\mathrm{p}}\mathbf{I} & k_{\mathrm{v}}R_{\mathrm{s}}\mathbf{I} \\ \mathbf{0} & \alpha_{\mathrm{f}}\mathbf{I} & -\alpha_{\mathrm{f}}\mathbf{I} \end{bmatrix}}_{\boldsymbol{A}_{\mathrm{c}}} \delta \boldsymbol{x}_{\mathrm{c}} \\ &+ \underbrace{\begin{bmatrix} -k_{\mathrm{i}}\mathbf{I} \\ k_{\mathrm{v}}(k_{\mathrm{p}} + r_{\mathrm{a}})\mathbf{I} \\ \mathbf{0} \end{bmatrix}}_{\boldsymbol{B}_{\mathrm{c}}} \delta \boldsymbol{i}_{\mathrm{s}} + \underbrace{\begin{bmatrix} \mathbf{0} \\ k_{\mathrm{v}}\mathbf{I} \\ \mathbf{0} \end{bmatrix}}_{\boldsymbol{B}_{\mathrm{u}}} \delta \boldsymbol{u}'_{\mathrm{s,ref}} \end{aligned} \tag{17a}$$

where $\delta \boldsymbol{x}_{\mathrm{c}} = \left[\delta \boldsymbol{w}_{\mathrm{i}}^{\mathrm{T}}, \delta \boldsymbol{i}_{\mathrm{s,ref}}^{\mathrm{T}}, \delta \boldsymbol{i}_{\mathrm{s,lpf}}^{\mathrm{T}}\right]^{\mathrm{T}}$ is the state vector of the controller, $\boldsymbol{i}_{\mathrm{s,ref}}$ is the voltage controller state variable (or the current reference), and $\boldsymbol{i}_{\mathrm{s,lpf}}$ is the state variable of the low-pass-filtered current reference. The input matrix $\boldsymbol{B}_{\mathrm{u}}$ provides an injection path for an additional voltage reference, i.e. for the compensator.

High-pass-filtered current reference is used in the voltage and frequency compensators. It is constructed using the low-pass-filtered current and its output matrix is

$$\delta \boldsymbol{i}_{\mathrm{s,hpf}} = \delta \boldsymbol{i}_{\mathrm{s,ref}} - \delta \boldsymbol{i}_{\mathrm{s,lpf}} = \underbrace{\begin{bmatrix} \mathbf{0} & \mathbf{I} & -\mathbf{I} \end{bmatrix}}_{\boldsymbol{C}_{\mathrm{f}}} \delta \boldsymbol{x}_{\mathrm{c}} \tag{17b}$$

The state matrix and the input matrices of the full electrical system are constructed from these two subsystems as

$$\frac{\mathrm{d}\delta\boldsymbol{x}}{\mathrm{d}t} = \underbrace{\begin{bmatrix} \boldsymbol{A} & \mathbf{0}_{4,6} \\ \boldsymbol{B}_\mathrm{c}\boldsymbol{C}_\mathrm{s} & \boldsymbol{A}_\mathrm{c} \end{bmatrix}}_{\boldsymbol{A}_\mathrm{t}} \delta\boldsymbol{x} + \underbrace{\begin{bmatrix} \boldsymbol{B}_\mathrm{s} \\ \mathbf{0}_{6,2} \end{bmatrix}}_{\boldsymbol{B}_\mathrm{S}} \delta\boldsymbol{u}_\mathrm{s} + \underbrace{\begin{bmatrix} \boldsymbol{b}_\mathrm{s} \\ \mathbf{0}_{6,1} \end{bmatrix}}_{\boldsymbol{b}_\mathrm{S}} \delta\omega_\mathrm{s}$$
$$+ \underbrace{\begin{bmatrix} \boldsymbol{b}_\mathrm{m} \\ \mathbf{0}_{6,1} \end{bmatrix}}_{\boldsymbol{b}_\mathrm{M}} \delta\omega_\mathrm{m} + \underbrace{\begin{bmatrix} \mathbf{0}_{4,2} \\ \boldsymbol{B}_\mathrm{u} \end{bmatrix}}_{\boldsymbol{B}_\mathrm{U}} \delta\boldsymbol{u}'_\mathrm{s,ref} \tag{18a}$$

where $\delta\boldsymbol{x} = [\delta\boldsymbol{x}_\mathrm{m}^\mathrm{T}, \delta\boldsymbol{x}_\mathrm{c}^\mathrm{T}]^\mathrm{T}$ is the combined state vector. The linearized output equations are extended as

$$\delta\boldsymbol{i}_\mathrm{s} = \underbrace{\begin{bmatrix} \boldsymbol{C}_\mathrm{s} & \mathbf{0}_{2,6} \end{bmatrix}}_{\boldsymbol{C}_\mathrm{S}} \delta\boldsymbol{x} \tag{18b}$$

$$\delta\tau_\mathrm{M} = \underbrace{\begin{bmatrix} \boldsymbol{c}_\mathrm{m} & \mathbf{0}_{1,6} \end{bmatrix}}_{\boldsymbol{c}_\mathrm{M}} \delta\boldsymbol{x} \tag{18c}$$

$$\delta\boldsymbol{i}_\mathrm{s,hpf} = \underbrace{\begin{bmatrix} \mathbf{0}_{2,4} & \boldsymbol{C}_\mathrm{f} \end{bmatrix}}_{\boldsymbol{C}_\mathrm{F}} \delta\boldsymbol{x} \tag{18d}$$

The control law (10) in matrix form is given by

$$\delta\boldsymbol{u}_\mathrm{s} = k_\mathrm{p}(\delta\boldsymbol{i}_\mathrm{s,ref} - \delta\boldsymbol{i}_\mathrm{s}) + \delta\boldsymbol{w}_\mathrm{i} - r_\mathrm{a}\delta\boldsymbol{i}_\mathrm{s} = -\boldsymbol{K}_\mathrm{c}\delta\boldsymbol{x} \tag{19}$$

where $\boldsymbol{K}_\mathrm{c} = \begin{bmatrix} (k_\mathrm{p} + r_\mathrm{a})\mathbf{I} & \mathbf{0} & -\mathbf{I} & -k_\mathrm{p}\mathbf{I} & \mathbf{0} \end{bmatrix}$. The control laws of the voltage and frequency injection compensators in (5) and (7) are gathered in matrix form, yielding

$$\begin{aligned} \delta\boldsymbol{u}_\mathrm{s,ref} &= -\left(\boldsymbol{K} + \mathbf{J}\psi_\mathrm{s0}\boldsymbol{k}^\mathrm{T}\right)\delta\boldsymbol{i}_\mathrm{s,hpf} \\ \delta\omega_\mathrm{s} &= -\boldsymbol{k}^\mathrm{T}\delta\boldsymbol{i}_\mathrm{s,hpf} \end{aligned} \tag{20}$$

The closed-loop system matrix $\boldsymbol{A}_\mathrm{T}$ of the electrical subsystem is acquired by inserting the linearized stator voltage control law (19) and the linearized control laws of the stator voltage and frequency injection compensators (20) into (18a), i.e.

$$\boldsymbol{A}_\mathrm{T} = \boldsymbol{A}_\mathrm{t} - \boldsymbol{B}_\mathrm{S}\boldsymbol{K}_\mathrm{c} - \left[\boldsymbol{B}_\mathrm{U}\left(\boldsymbol{K} + \mathbf{J}\psi_\mathrm{s0}\boldsymbol{k}^\mathrm{T}\right) + \boldsymbol{b}_\mathrm{S}\boldsymbol{k}^\mathrm{T}\right]\boldsymbol{C}_\mathrm{F} \tag{21}$$

Finally, the overall system matrix is obtained by interconnecting the electrical and the mechanical subsystems

$$\boldsymbol{A}_\mathrm{F} = \begin{bmatrix} \boldsymbol{A}_\mathrm{T} & \boldsymbol{b}_\mathrm{M} \\ \boldsymbol{c}_\mathrm{M}/J_\mathrm{m} & 0 \end{bmatrix} \tag{22}$$

C. Stability Analysis

The stability of the current-regulated V/Hz control method is analyzed by studying the eigenvalues of the overall system matrix of the current-regulated V/Hz control in (22). It is revealed, that the real part of the pole-pair corresponding to the current controller is placed at $-\alpha_\mathrm{c}$ and the real part of the pole-pair corresponding to voltage controller is placed at $-\alpha_\mathrm{u}$ when the voltage controller integral gain is selected as

$$k_\mathrm{v} = \frac{\alpha_\mathrm{u} - \alpha_\mathrm{c}}{\alpha_\mathrm{c}L_\sigma} \tag{23}$$

Next, the effect of the voltage integral gain is studied. In Fig. 3, the eigenvalues of the system matrix corresponding to the open-loop V/Hz-controlled induction motor [4] (shown in red) are compared to the eigenvalues of the current-regulated V/Hz controlled system in (22) for varying choices for α_u (shown in blue). Only the upper half-plane poles relevant for system stability are shown due to symmetry.

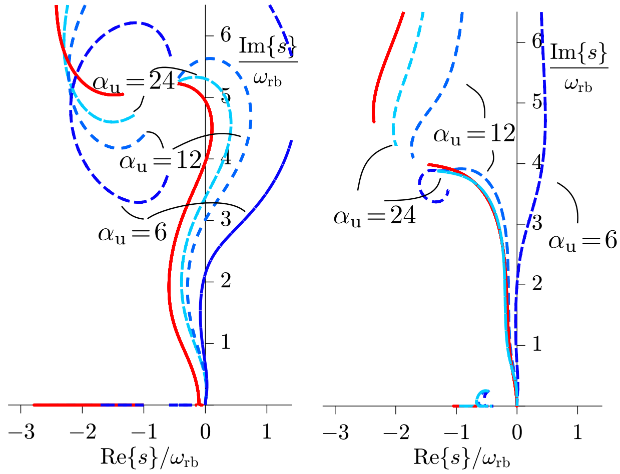

(a) (b)

Fig. 3. Root loci of the system defined in (22) using the parameters of the 45-kW induction motor in no-load condition as stator frequency ω_s0 varies. In (a) the static feedback compensation is disabled ($\boldsymbol{K} = \mathbf{0}, \boldsymbol{k} = 0$) and in (b) enabled ($k = 0.6$ and $k_\omega = 4$). The red loci corresponds to V/Hz controlled induction motor in [4], and the blue corresponds to current-regulated V/Hz control with varying voltage controller integral gains ($\alpha_\mathrm{u} = 6$ p.u., $\alpha_\mathrm{u} = 12$ p.u and $\alpha_\mathrm{u} = 24$ p.u). Current controller bandwidth is kept constant ($\alpha_\mathrm{c} = 3$ p.u.).

In Fig. 3a the feedback compensation is disabled ($\boldsymbol{K} = \mathbf{0}, \boldsymbol{k} = 0$). As the gain k_v or the ratio $\alpha_\mathrm{u}/\alpha_\mathrm{c}$ is increased, the dominating poles move towards the left half-plane and the location of the corresponding poles of open-loop V/Hz control.

Fig. 3b, shows the system eigenvalues with the static feedback compensation enabled. The red loci corresponds to the poles of the V/Hz controlled induction motor with static feedback compensation described in [4] ($k = 0.6$ and $k_\omega = 4$). The blue loci present the eigenvalues of the current-regulated V/Hz control method with the same stabilizing feedback gains for varying choices for α_u

Without the stabilizing feedback in (5) and (7), the current-regulated V/Hz control scheme exhibits regions of instability. As the voltage controller gain is increased, the unstable region shrinks approaching that found in open-loop V/Hz control. Insufficient gain in the voltage controller will also result in an unstable region remaining, even with the stabilization enabled. The maximum limiting factor for choosing a value for the integral gain k_v is the angular sampling frequency, i.e. the pole pair at α_u cannot be placed too close to it.

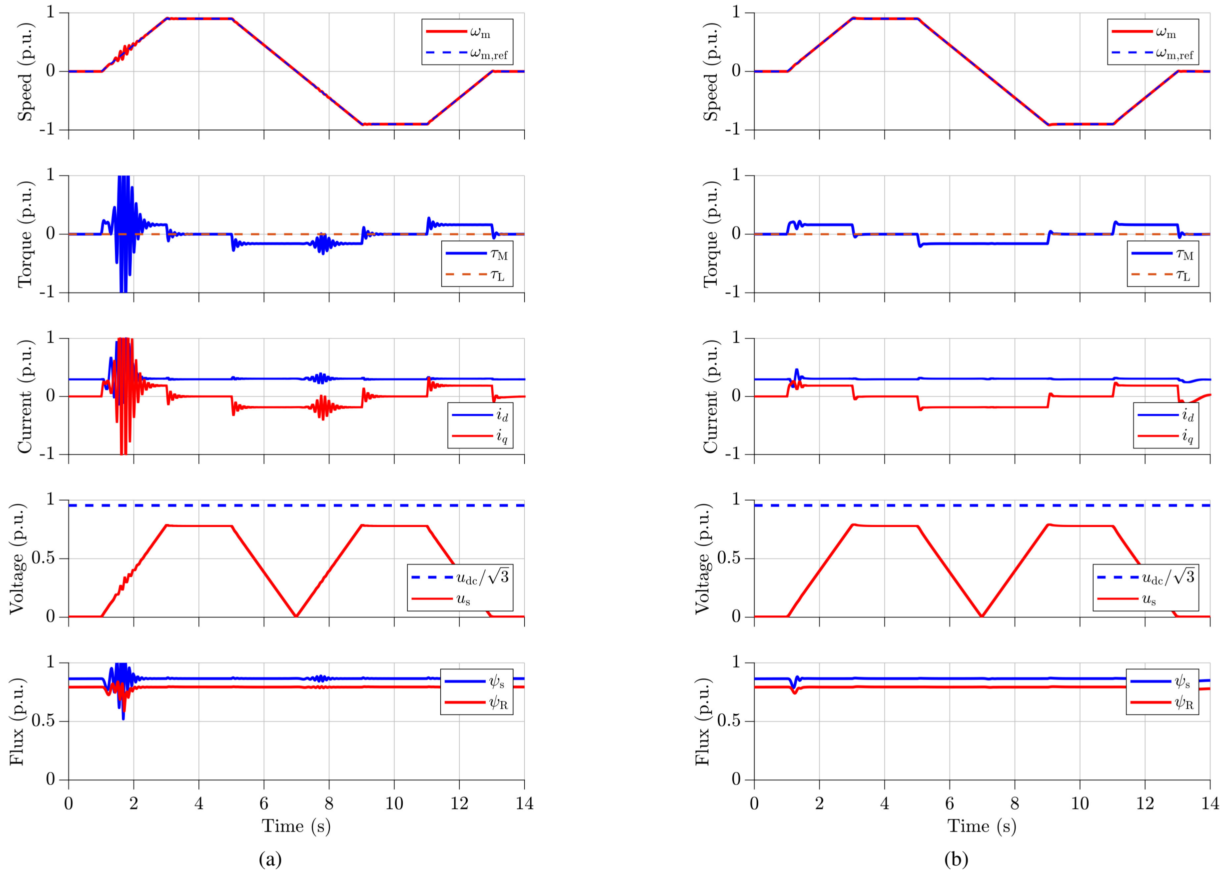

Fig. 4. Simulation result: Speed reference is first increased to 0.9 p.u. and then reversed to -0.9 p.u. Fig. 4a shows current-regulated V/Hz control without compensation loops and Fig. 4b current-regulated V/Hz control with the compensation feedback enabled ($k_\mathrm{v} = 0.6, k_\omega = 4$). In both cases, the current controller bandwidth is $\alpha_\mathrm{c} = 3$ p.u. and the voltage controller integral gain is set according to (23) with $\alpha_\mathrm{u} = 4 \cdot \alpha_\mathrm{c} = 12$ p.u.

TABLE I
DATA OF THE 45-KW FOUR-POLE INDUCTION MOTOR

Rated values		
Voltage (line-to-neutral, peak value)	$\sqrt{2/3}{\cdot}400$ V	1 p.u.
Current (peak value)	$\sqrt{2}{\cdot}81$ A	1 p.u.
Frequency	50 Hz	1 p.u.
Speed	1 477 r/min	0.985 p.u.
Torque	291 Nm	0.81 p.u.
Parameters		
Stator resistance R_s	60 mΩ	0.02 p.u.
Rotor resistance R_R	30 mΩ	0.01 p.u.
Leakage inductance L_σ	2.2 mH	0.24 p.u.
Magnetizing inductance L_M	24.5 mH	2.70 p.u.
Rotor inertia J_r	0.49 kgm^2	67.4 p.u.

V. RESULTS

The current-regulated voltage controlled V/Hz control method is studied with simulations and experiments. A four-pole 400-V 50-Hz 45-kW induction motor is used as an example motor, whose parameters and rated values of the motor are given in Table I. Fig. 7 shows a photo of the motor test bench used in the experiments. The control algorithm was implemented on a dSPACE MicroLabBox prototyping system. The switching and the sampling frequency of the PWM inverter are both 4kHz. The current-controller bandwidth is selected as $\alpha_\mathrm{c} = 3$ p.u. and integral gain of the voltage controller is selected according to (23) with $\alpha_\mathrm{u} = 4\alpha_\mathrm{c}$. The bandwidth of the low-pass current filter is $\alpha_\mathrm{f} = 1/50$ p.u. For the stabilizing feedback, the voltage injection gain is selected as $k_\mathrm{u} = 0.6$ and the frequency injection gain as $k_\omega = 4$. The induction motor is magnetized on startup with nominal magnetizing current.

A. Simulations

Fig. 4 shows a simulation result where the speed reference is ramped from zero to 0.9 p.u. and then reversed to -0.9 p.u. and finally brought back to zero. The load torque is zero. Fig. 4a presents the results for current-regulated V/Hz without stabilizing feedback enabled corresponding to the method presented in [10]. The motor is pre-magnetized on startup. As suggested by the stability analysis in Section IV-C, the system is unstable in the middle-speed region ($\omega_\mathrm{s} \approx \pm 0.2$ p.u.) and the dampening is poor. Fig. 4b shows the same sequence with the stabilizing feedback enabled. The oscillations in the middle-speed region are removed and the damping is significantly improved.

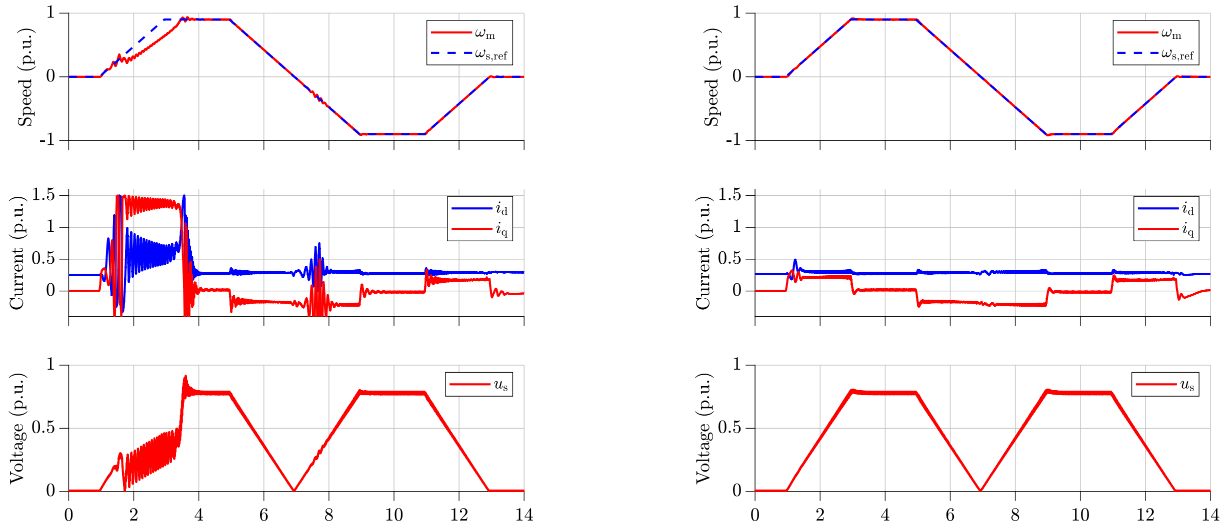

(a) (b)

Fig. 5. Experimental result: Speed reference is increased to 0.9 p.u., then reversed to -0.9 p.u. and finally brought back to zero.In Fig. 5a the compensation feedback is disabled, and in Fig. 5b it is enabled ($k_{\mathrm{v}} = 0.6, k_{\omega} = 4$).

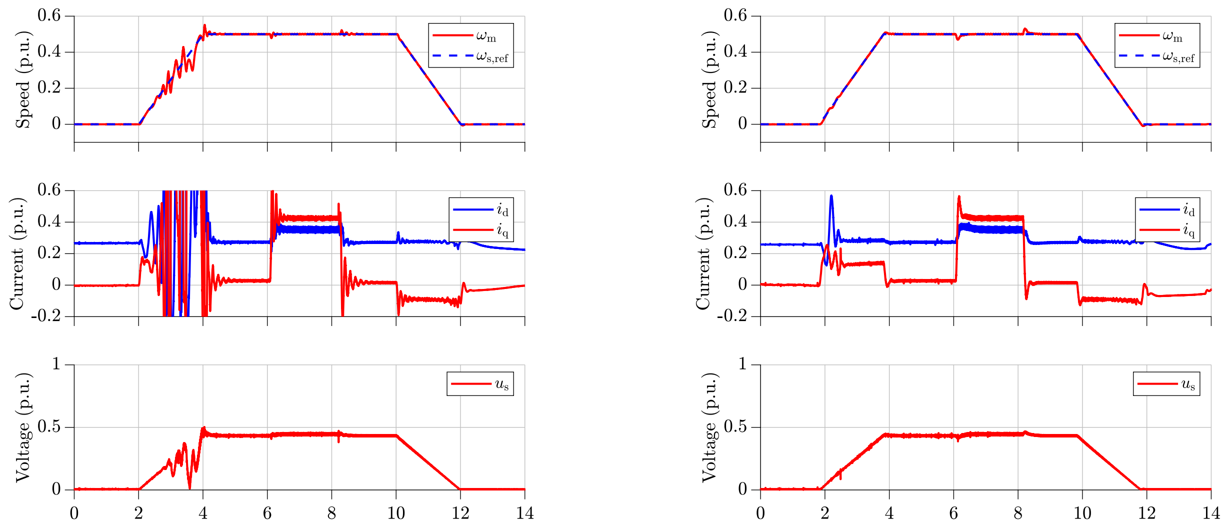

(a) (b)

Fig. 6. Experimental result: Speed reference is increased to 0.5 p.u. From $t = 6$ s to $t = 8$ s, a loadstep of 0.5 p.u. is applied. In Fig. 6a the compensation feedback is disabled, and in Fig. 6b it is enabled ($k_{\mathrm{v}} = 0.6, k_{\omega} = 4$).

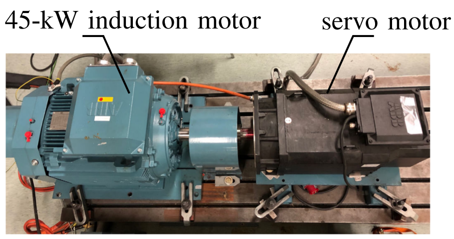

Fig. 7. Photo of the motor test bench. The analyzed 45-kW induction motor is on the left. The 37-kW induction servo motor on the right-hand side is used as a load machine.

B. Experiments

Fig. 5 shows an experiment with a sequence similar to the simulation sequence in Fig. 4. In Fig. 5a the static feedback compensation is disabled. Again, the drive becomes unstable upon reaching the unstable mid-speed region. The magnitude of the oscillations in the experiments surpasses those seen in the simulations. Stability is regained after the unstable region around $t = 3$. In addition to the unstable regions, the system exhibits poor damping. In Fig. 5b, the experiment is repeated with the compensation enabled. The system is stable and well damped.

Next, in Fig. 6, the speed reference is set to 0.5 p.u. Then, at $t = 6$ s, a load torque 0.5 p.u. is applied for a duration of 2 seconds. At $t = 10$ the speed is reduced back to zero. The slip compensator corrects the speed error. In Fig. 6a, the stabilizing feedback compensation is disabled. In addition to the instability during acceleration, poor damping is observed. The oscillations last for almost a second after a stepwise change in load torque. Fig. 6b shows a repeat of the same sequence, but this time the compensation feedback is enabled. The damping in the transient response is visibly improved.

VI. Conclusions

The paper analyzed a V/Hz control method consisting of an inner current control loop and an outer voltage control loop. It is shown, that similarly to conventional open-loop V/Hz control, this current-regulated V/Hz control method exhibits regions of instability and poor damping. Consequently, in this paper, the current-regulated V/Hz control is enhanced with stator resistance and slip-compensation loops and stabilizing static output feedback, which is used to increase the stable operating region and damping. Compared to conventional V/Hz with stabilizing loops, the added current controller can be utilized e.g. in current limitation. Furthermore, magnetization of the machine can be easily achieved if the rated magnetizing current is known.

References

[1] A. Munoz-Garcia, T. Lipo, and D. Novotny, "A new induction motor v/f control method capable of high-performance regulation at low speeds," *IEEE Transactions on Industry Applications*, vol. 34, no. 4, pp. 813–821, 1998.

[2] O. E.-S. Mohammed Youssef, "A new open-loop volts/hertz control method for induction motors," in *2018 Twentieth International Middle East Power Systems Conference (MEPCON)*, 2018, pp. 266–270.

[3] A. Smith, S. Gadoue, M. Armstrong, and J. Finch, "Improved method for the scalar control of induction motor drives," *IET Electric Power Applications*, vol. 7, no. 6, pp. 487–498, 2013. [Online]. Available: https://ietresearch.onlinelibrary.wiley.com/doi/abs/10.1049/iet-epa.2012.0384

[4] M. Hinkkanen, L. Tiitinen, E. Mölsä, and L. Harnefors, "On the stability of volts-per-hertz control for induction motors," *IEEE Journal of Emerging and Selected Topics in Power Electronics*, pp. 1–1, 2021.

[5] T. A. Lipo and P. C. Krause, "Stability analysis of a rectifier-inverter induction motor drive," *IEEE Transactions on Power Apparatus and Systems*, vol. PAS-88, no. 1, pp. 55–66, 1969.

[6] Y. Liu and B. Piepenbreier, "Improvement of dynamic characteristic for v/f controlled induction motor drive system," in *2014 International Symposium on Power Electronics, Electrical Drives, Automation and Motion*, 2014, pp. 707–712.

[7] G.-J. Jo and J.-W. Choi, "Rotor field-oriented drive system implementation with oscillation suppression compensator in induction motors," *IEEE Journal of Emerging and Selected Topics in Power Electronics*, vol. 9, no. 3, pp. 2745–2758, 2021.

[8] O. E.-S. Mohammed Youssef, "A New Open-Loop Volts/Hertz Control Method for Induction Motors," in *2018 Twentieth International Middle East Power Systems Conference (MEPCON)*, 2018, pp. 266–270.

[9] M. Kutija, D. Sumina, and I. Čolović, "A current limiting technique for v/f controlled induction machines," in *2014 16th International Power Electronics and Motion Control Conference and Exposition*, 2014, pp. 1001–1004.

[10] R. Kerkman and T. Rowan, "Voltage-controlled current-regulated pwm inverters (for motor drive applications)," *IEEE Transactions on Industry Applications*, vol. 26, no. 2, pp. 244–251, 1990.

[11] G. R. Slemon, "Modelling of induction machines for electric drives," *IEEE Transactions on Industry Applications*, vol. 25, no. 6, pp. 1126–1131, Nov./Dec. 1989.

[12] L. Harnefors and H.-P. Nee, "Model-based current control of AC machines using the internal model control method," *IEEE Trans. Ind. Appl.*, vol. 34, no. 1, pp. 133–141, Jan./Feb. 1998.

Lauri Tiitinen received the B.Sc.(Tech.) and M.Sc.(Tech.) degrees in electrical engineering from the Aalto University, Espoo, Finland, in 2019 and 2020, respectively. He is currently working toward the D.Sc.(Tech.) at Aalto University. His research interests include control and self-commissioning of electric motor drives.

Floran Martin received the Engineering Diploma in electrical engineering from Polytech Nantes, Nantes, France, in 2009, and the M.S. and Ph.D. degrees in electrical engineering from the University of Nantes, Nantes, in 2009 and 2013, respectively. In 2014, he joined the Department of Electrical Engineering and Automation, Aalto University, Espoo, Finland, where he is currently a Staff Scientist. His research interests include modeling of magnetic materials as well as analyzing, designing, and controlling electrical machines.

Marko Hinkkanen (Senior Member, IEEE) received the M.Sc.(Eng.) and D.Sc.(Tech.) degrees in electrical engineering from the Helsinki University of Technology, Espoo, Finland, in 2000 and 2004, respectively.

He is currently an Associate Professor with the School of Electrical Engineering, Aalto University, Espoo, Finland. His research interests include control systems, electric drives, and power converters.

Dr. Hinkkanen was a General Co-Chair for the 2018 IEEE 9th International Symposium on Sensorless Control for Electrical Drives (SLED). He was the corecipient of the 2016 International Conference on Electrical Machines (ICEM) Brian J. Chalmers Best Paper Award, the 2016 and 2018 IEEE Industry Applications Society Industrial Drives Committee Best Paper Awards, and the 2020 SEMIKRON Innovation Award. He is an Associate Editor for the IEEE TRANSACTIONS ON ENERGY CONVERSION and the *IET Electric Power Applications*.

Lennart Harnefors (Fellow, IEEE) received the M.Sc., Licentiate, and Ph.D. degrees in electrical engineering from the Royal Institute of Technology (KTH), Stockholm, Sweden, and the Docent (D.Sc.) degree in industrial automation from Lund University, Lund, Sweden, in 1993, 1995, 1997, and 2000, respectively.

From 1994 to 2005, he was with Mälardalen University, Västerås, Sweden, from 2001 as a Professor of electrical engineering. From 2001 to 2005, he was, in addition, a part-time Visiting Professor of electrical drives with Chalmers University of Technology, Göteborg, Sweden. In 2005, he joined ABB, HVDC Product Group, Ludvika, Sweden, where, among other duties, he led the control development of the first generation of multilevel-converter HVDC Light. In 2012, he joined ABB, Corporate Research, Västerås, where he was appointed as a Senior Principal Scientist in 2013. He is, in addition, a part-time Adjunct Professor of power electronics with KTH.

Dr. Harnefors is an Editor for the IEEE JOURNAL OF EMERGING AND SELECTED TOPICS IN POWER ELECTRONICS and an Associate Editor for the *IET Electric Power Applications*. He was the recipient of the 2020 IEEE Modeling and Control Technical Achieved Award and was acknowledged as an outstanding reviewer of IEEE TRANSACTIONS OF POWER ELECTRONICS in 2018. His research interests include control and dynamic analysis of power electronic systems, particularly grid-connected converters and ac drives.